Cell morphology as a quantifier for functional states of resident tissue macrophages

Miriam Schnitzerlein[1,2], Anja Wegner[3,4,5], Oumaima Ben Brahim[3,4,5], Stefan Uderhardt[3,4,5*], Vasily Zaburdaev[1,2*]

1 Department of Biology, Friedrich-Alexander-Universität Erlangen-Nürnberg, 91058 Erlangen, Germany
2 Max-Planck-Zentrum für Physik und Medizin, 91058 Erlangen, Germany
3 Department of Medicine 3 - Rheumatology and Immunology, Friedrich-Alexander-Universität Erlangen-Nürnberg (FAU) and Universitätsklinikum Erlangen, 91054 Erlangen, Germany
4 Deutsches Zentrum für Immuntherapie, FAU, 91054 Erlangen, Germany
5 Exploratory Research Unit, Optical Imaging Competence Center Erlangen, FAU, 91058 Erlangen, Germany

* stefan.uderhardt@fau.de, vasily.zaburdaev@fau.de

Abstract

Resident tissue macrophages (RTMs) are essential for maintaining homeostasis in a physiological tissue state. They monitor interstitial fluids, contain acute damage while actively preventing inflammation, and remove dead cells and debris. All these cellular functions are accompanied by characteristic changes in cell morphology, the expression of which can provide information about the functional status of the cells. What is currently known about morphological patterns and dynamic behavior of macrophages is derived primarily from experimental *ex vivo* cell cultures. However, how macrophages operate in living organisms is in many ways fundamentally different from how they do in a cell culture system. In this work, we employed an intravital imaging platform to generate dynamic data from peritoneal RTMs *in vivo* in mice under various conditions induced either chemically or physically. Using this data, we built an image processing pipeline and defined a set of human-interpretable cell size and shape features which allowed us to quantify RTM morphodynamics over time. We used those features to quantitatively differentiate cells in various functional states - when macrophages are activated, for instance, or when they "shut down" due to detrimental changes in the environment. The qualitative morphology changes associated with these functional states could be inferred directly from the quantitative measurements. Finally we used the set of cell morphology features monitoring the health of RTMs to improve a setup for explanted tissues. Thus, the proposed method is a versatile tool to provide insights into the dynamic behavior of *bona fide* macrophages *in vivo* and helps distinguish between physiological and pathological cell states.

Author summary

Mammalian tissues are constantly subjected to various stresses - due to pathogens, cell death and molecular waste products - which have to be resolved properly to prevent unwanted inflammatory processes and thus maintain tissue homeostasis. To find such

incidents, resident tissue macrophages (RTMs) *in vivo* display constant sampling behavior which is accompanied by dynamic changes to their morphology. These changes of cellular features are not yet fully understood and were even not yet quantified for RTMs in living organisms. To fill this knowledge gap, we have used an intravital imaging platform to generate time-lapse images of RTMs over time in the peritoneal serosa of a living mouse. Subsequently we have built a custom image processing pipeline to assess the morphology and dynamics of the cells. We could use these measurements to recover the qualitative cell morphology changes over time and even differentiate cells in distinct physiological and pathological states. Thus this analysis lays the basis to the further development of a mathematical model or RTM sampling dynamics or may even be the first step to diagnose macrophages in disease contexts.

Introduction

Resident tissue macrophages (RTM) are the most common immune cell type found in healthy mammalian organs and tissues [1]. On the one hand, depending on the niche they occupy, they perform vital tissue-specific tasks, like microglia in the brain which prune synapses, alveolar macrophages in the lungs which regulate the turnover of surfactant and lipids, or macrophages of the red pulp of the spleen which dispose of aged erythrocytes [2–4]. On the other hand, RTMs perform general core functions that are independent of their host organ. These include the pinocytotic surveillance of interstitial fluids [5], the anti-inflammatory containment of acute damage ("cloaking") [6] as well as the professional removal of dead cells and debris [7], maintaining an overall homeostatic state required for regular tissue function. These functions, as well as the polarization and activity state of macrophages, are characterized by dynamic changes in cell morphology, some of which can be reproduced in cell culture systems using bone marrow-derived macrophages (BMDM). However, RTM are fundamentally different from BMDM in that they are sessile and firmly attached to their surrounding matrix scaffold. Therefore, differentiated interstitial RTMs generally do not migrate through tissues but perform their functions locally in the interstitial space around them, unrestricted by the two-dimensional plane of cell culture. Their morphologies and dynamic behaviors hence differ considerably, reflecting the physiological requirements and anatomical constraints of the individual niche. A particular dynamic behavior of RTM *in vivo* is tissue surveillance by pinocytic sampling, manifested by the recurrent formation of prominent membrane protrusions and the uptake of larger amounts of interstitial fluid. Critically, we have previously established a qualitative relationship between macrophage morphology and functional core functions such as sampling or cloaking imperative for tissue homeostasis [5]. A quantitative understanding of the morphodynamics of RTMs *in vivo* is the basis for developing mathematical models capable of predicting both the activation and functional state of RTMs *in situ* based on optical imaging data. Combined with further profiling approaches, this will enable us to more accurately diagnose macrophage dysfunction in a spatial context and better explain pathological processes at the tissue level.

The analysis of cell morphologies to distinguish and detect different cell types as well as to directly detect functional states of cells, their proliferation patterns, locomotion and migratory behavior is a rapidly growing research area [8–11]. The general concept of a broad range of shape-quantification methods is to reduce generally very complex cell shapes into a small number of easily interpretable quantifiers that can be used to distinguish cells according to the research questions, e.g., their phenotype or state of activation. Although cell shape analyses have been used to characterize macrophages under various conditions, most of the approaches used were either not designed to assess the dynamic behavior of peripheral RTMs over time or did not take into account the

inherent characteristics of sessile RTMs *in vivo*. Therefore, further studies are needed that capture and quantitatively analyze the behavior of peripheral RTMs over time, their natural shape, and their dynamic adaptations in a living tissue with high spatial and temporal resolution.

Here, we use an established intravital imaging platform to generate dynamic data from murine RTMs of the peritoneal serosa *in vivo*, under steady-state resting conditions and upon chemical or physical perturbation. To analyze this data and quantify RTM morphodynamics over time, we built an image processing pipeline for which we defined a set of human-interpretable cell size and shape features. These analyses provided unprecedented insight into the dynamic behavior of RTMs within a living tissue and revealed quantifiers that could distinguish between physical and pathological cell states and infer qualitative morphological changes from the quantitative measurements. Specifically, we were able to quantitatively assess how RTMs contract and become passive when their sampling activity was compromised by chemical stimuli. Our morphometric analysis approach also provides the basis for the informed development of novel tissue culture systems and explant platforms in which macrophage functions can be preserved and studied as closely as possible to the situation in the living organism.

Results

Macrophages *in vivo* and *in vitro* display different morphodynamics

Functionally, RTMs are a product of their immediate environment and anatomical conditions, as evidenced by the variety of possible morphological expressions. Outside the body, they rapidly lose this expression and morphologically reorient to the conditions of the particular culture system, either within a 3D biological matrix or along the 2D culture dish surface. Macrophages *in vivo* therefore differ fundamentally in their morphodynamics from macrophages *ex vivo*. Bone marrow-derived macrophages (BMDMs), for instance, show two main morphologies: on the one hand, there are cells with a mesenchymal migration mode characterized by a moving, leading edge on one side, with the nucleus trailing on the opposite side of the cell. On the other hand, there are migrating BMDMs with a more round cell body with very long and thin appendages and protrusions (see Fig 1 A, B).

In stark contrast, RTMs visualized using our *in vivo* peritoneal imaging platform (see Materials and Methods) behaved quite differently and exhibited a more complex shape consisting of an immobile cell body with multiple, thicker dynamic protrusions as visible in Fig 1 C. These cells were stationary and probed their surrounding environment by extending and retracting their protrusions rather than migrating through the tissue themselves, as shown in Fig 1 D. Here, the cell retracts the protrusion at the upper right over time (marked by light green arrow) and builds a new one at the upper left (marked by a dark green arrow), while only (slightly) remodeling the two protrusions at the bottom (marked by purple arrows). The center of mass of its main cell body remains thereby stationary as visualised by the light blue, dashed line.

In summary, macrophages outside a tissue, such as *in vitro*-generated BMDMs, are migratory cells, whereas RTMs *in vivo* are sessile cells with a complex shape that exhibit dynamic behavior through the movement of their protrusions. Since cell morphology can be related to cell function, we sought to quantitatively analyze RTM shapes *in vivo* over time.

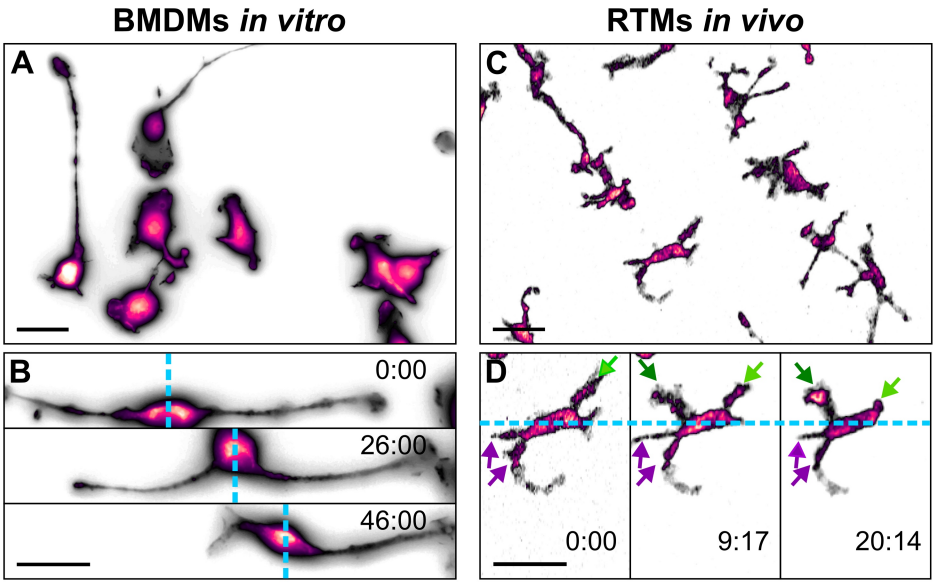

Fig 1. Comparison of BMDMs *in vitro* with peritoneal RTMs *in vivo*. (A) Overview of BMDMs imaged in a flat cell culture system - the corresponding movie is provided in S1 Video. (B) Snapshots of a migrating BMDM over time. (C) Overview of RTMs imaged *in vivo* in the peritoneal serosa of a mouse - the corresponding movie is provided in S2 Video. (D) Snapshots of a single stationary RTM showing sampling activities over time, protrusions are marked by arrows. The light blue line(s) illustrate the center of mass of the specific cells. All scale bars equate to 30 µm; the time is given as minutes:seconds.

Cell shape features quantitatively describe RTM morphology changes

The sampling dynamics exhibited by RTMs during their surveillance behavior have a visible impact on the overall morphology of cells over time. Therefore, by assessing and analyzing cell size and shape over time it is possible to characterize one of the biological core functions of RTMs *in vivo*. We acquired three-dimensional, intravital images of the peritoneal serosa of living mice over time, which were then corrected for jittering or drifts (see Materials and Methods for details). Due to the geometry of the submesothelial compartment of the peritoneum, RTMs here operate almost exclusively parallel to the surface area, without extending protrusion along the z-axis. Thus it was justified to use 2D images obtained by maximum intensity projection, which also allowed us to increase the through-put and simplify further analysis. A representative sample image of a macrophage is shown in Fig 2 A, from which then the cell morphology and dynamics is analyzed.

There are many different methods to quantify cell shapes, which can be subdivided into broad categories [8, 12, 13]. First, a certain shape can be characterized by the location of a set of individual 'landmark points', which are distinct structures on the shape commonly set by hand. While most cells do not display such specific and consistent features - in contrast to e.g. organs or whole organisms - for specific cell types like neurons critical points could be defined as the end points and junctions of a single neurite [14].

Secondly, the outline of a segmented cell can be described implicitly by using a geometrical representation employing e.g. a 'signed distance map', 'level sets' or Fourier descriptors. In [15], Fourier descriptors were used to characterize unique cell shapes of

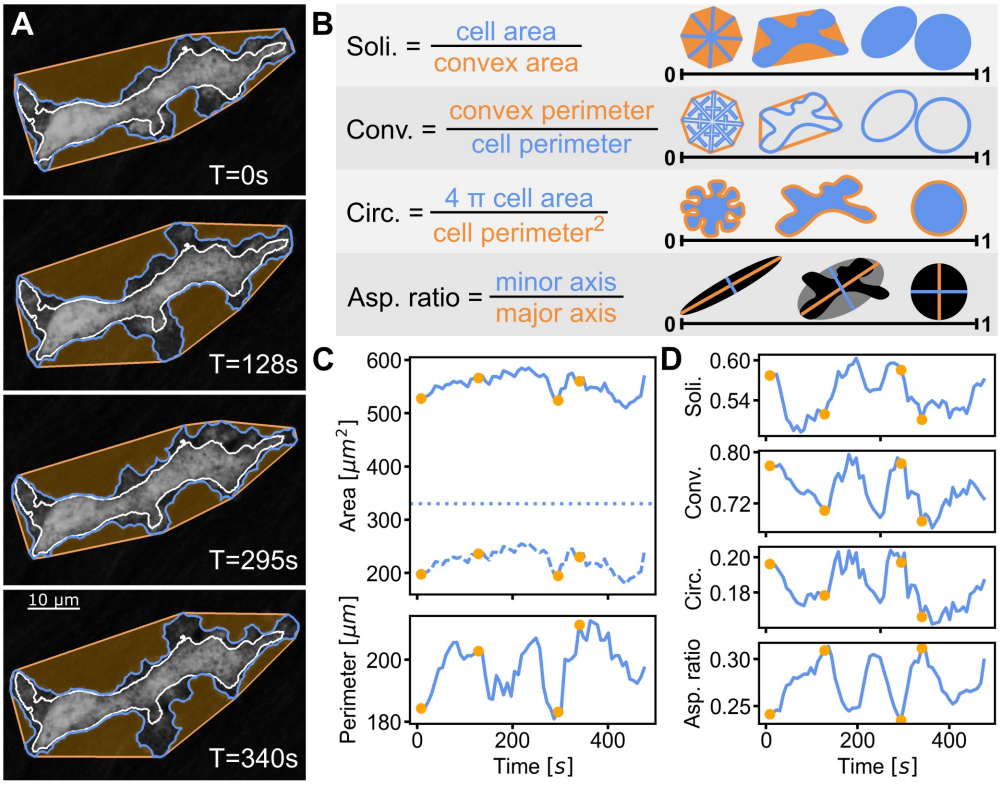

Fig 2. Visualization of cell size and cell shape for a single exemplary RTM over time. (A) Snapshots of an RTM at representative time points with marked outline of fixed area (white), outline of whole cell (cornflowerblue) and outline of convex hull (orange). (B) Definition of cell shape parameters and corresponding sketches qualitatively visualizing potential cell shapes. (C) Cell size of the exemplary cell from (A) over time. On top: Whole cell area, mobile cell area (dashed) and fixed cell area (dotted). On bottom: Perimeter. (D) Cell size quantifiers over time for the exemplary cell from (A); from top to bottom: Solidity, Convexity, Circularity, Aspect ratio. (C, D) The time points of the movie snapshots are marked with an orange dot on the time series.

D.discoideum as they were migrating due to different chemical stimuli.

Finally, the overall shape of a cell can be described by measuring a set of human-interpretable 'features', which may include cell area (volume) and perimeter (surface area), the lengths of the minor and major axis, circularity or solidity [12, 13]. Such features can be extracted in a highly automated manner and have been used before to analyze specifically macrophages in varying contexts. To study brain injury, microglia in fixed mouse brain samples were analyzed regarding their area, solidity and aspect ratio, thereby describing how cells change their shape due to applied trauma [16]. In [17], the elongation of macrophages was measured and subsequently correlated with their chemically induced polarization. Similarly, the eccentricity of macrophages was used in [18] to build an automated, high-throughput assessment pipeline to differentiate between differently activated macrophages cultivated in a cell culture system. To describe the morphology of RTMs, we use quantifiers of the overall cell shape which can be divided into features describing specifically the cell size and features describing the cell shape as visualized in Fig 2 B. Extracting and analyzing the features is implemented in a custom pipeline, as described in the Methods section. To quantify cell

size, the area of the 2D-projection of the cell as well as the corresponding perimeter were measured. The area of the cell can, however, be split into two subtypes. We have previously shown that RTMs of the submesothelial peritoneum are sessile and nonmigratory cells that are firmly attached to the surrounding extracellular matrix at yet uncharacterized anchor sites [6]. We determined the **fixed** area by integrating the movie over time and subsequently applying a threshold of 97% which removed lower intensity parts corresponding to temporal protrusions. The remaining cell area after subtracting the fixed area from the whole area is termed **mobile** area. The evolution of cell size parameters over time is plotted for a representative example cell in Fig 2 C.

There are four cell shape parameters chosen here: The solidity of a cell is the ratio of the cell area to its convex area; it measures how spread-out the cell is. The ratio of the convex perimeter to the cell perimeter is called convexity and evaluates how 'wrinkly' the cell outline is. The circularity of the cell assesses how close a shape resembles a circle and is calculated from the ratio of cell area and cell perimeter. The aspect ratio is the ratio of the minor to the major axis of the cell shape and quantifies the elongation of the cell. All of these cell shape quantifiers range from 0 to 1 and are qualitatively explained for different shapes in Fig 2 B. These quantifiers are easily interpretable and thus enable us to make statements about the overall cell shape changes by tracking these values as a function of time, see Fig 2 D.

The cell shown in Fig 2 A was actively sampling in a resting state, i.e., not activated by external stimuli, and probably at or near its physiological equilibrium. There were no long-term trends apparent in the cell behavior. This indicated that, first of all, the imaging protocol itself did not affect the morphology or dynamics of the cell. Secondly, this demonstrated that the image processing pipeline is robust in a sense that - even though the fluorescence intensity was decreasing over time due to photobleaching (see S1 Fig) - the cell segmentation and subsequent assessment of cell morphology features was consistent over the whole duration of observation.

We found that the changes of the cell size and shape quantifiers (Fig 2 C, D) were fluctuating within a relatively narrow range, e.g. $\leq 15\%$ for the perimeter, while the cell morphology was still visibly changing (compare panels 1 and 2 of Fig 2 A). These cell morphology changes were due to the expansion (Fig 2 A, panel 2 and 4) and retraction (Fig 2 A, panel 1 and 3) of the cell protrusions, which occurred almost cyclically. This periodic behavior describing the sampling activity of RTMs was recovered in the measurements of the cell shape over time, see for example the aspect ratio (Fig 2 D, bottom plot).

Having shown that our chosen parameters can reliably quantify the equilibrium state of RTMs, the features were tested to successfully discriminate between RTMs exposed to different chemical stimuli and therefore in different functional cell states. For that, the time series of each single feature needed to be summarized into a discrete value describing the morphology and dynamics of the macrophages independent of time.

Morphology quantifiers discriminate between RTMs in physiological and pathological cell states

To summarize the cell morphology quantifiers for a given cell and to facilitate comparison of RTMs outside of their physiological equilibrium, summary statistics were introduced to reduce the measurements of the different cell size and shape quantifiers over time to single parameter values per cell. The mean of the features provides information about the average cell morphology, while the standard deviation of these features reveals insights into the dynamics of RTMs. Finally, the trend of the data - measured as the slope of a linear fit to the time series - indicated whether the cells were either still actively adapting to (new) environmental stimuli or whether morphological

polarization was already complete.

To test how sensitive the different quantifiers are to cell morphology changes of RTMs in different cell states, the cells were exposed to four different stimuli (see Methods). Lipopolysaccharide (LPS), which is part of the bacterial cell wall and triggers macrophages to induce an acute inflammatory response [19]. The signaling factor Macrophage Colony Stimulating Factor (M-CSF) is a differentiation factor for macrophage precursors which, among other things, enhances the endocytotic activity of macrophages [20]. At the end of the imaging experiments, the mice were euthanized with isoflurane (Iso) as a sedative in overdose - this allowed us to additionally investigate the changes in the behavior of the RTMs during tissue hypoxia due to respiratory insufficiency. Lastly YM201636 (YM) is an inhibitor of the kinase PIKfyve which abrogated endosomal resolution and thus shut down sampling dynamics without affecting acute cell viability [5, 21]. The imaging data for this experiment was thereby taken from [5]. Representative snapshots of RTMs *in vivo* subjected to the perturbations are shown in Fig 3 A.

All parameters described above were analyzed for the cell populations under the five different cell states, one control (Ctrl) and four perturbations (LPS, M-CSF, Iso, YM) and their detailed comparison can be found in S2 Fig-S4 Fig. We found that certain cell morphology parameters, such as the mean perimeter or the standard deviation of the solidity of RTMs, were suitable to differentiate between different conditions (Fig 3 B, C) while other parameters - like the trend of aspect ratio or the standard deviation of circularity - showed no significant differences when comparing whole cell populations with each other (Fig 3 D, E).

However, the design of the experimental imaging platform allowed us to compare the cells before and after treatment, which provided a direct comparison of the different behaviors of the same cells. Thus, when the morphology of a RTM cell was first analyzed in a resting state and was then compared to the morphology of the same cell after or under chemical stimulation, the parameters of the trend of aspect ratio or the standard deviation of circularity could in fact differentiate between control and M-CSF-activated cells (Fig 3 F , G).

We have shown that our set of parameters were indeed capable of differentiating between RTMs perturbed by different chemical stimuli - some of the features do so on the population-level while others are more useful in direct comparison at the cell-level. Next, we took advantage of selecting human-interpretable features to infer qualitative changes in cell morphology and dynamics from quantitative measurements.

Qualitative morphology changes of RTMs can be deduced from quantitative cell shape measurements

From our quantitative measurements, the overall qualitative cell morphology and dynamics changes for a cell population under a certain condition could be deduced. For RTMs acutely treated with **LPS** no immediate morphological changes could be determined, neither visually nor given our quantitative parameters. In other studies, where cells were stimulated with LPS for 24 hours, RTMs were spread over a larger area and had more filopodia [22, 23]. Thus, morphological changes in RTMs might be a long-term effect of LPS stimulation, which were not evident upon short-term stimulation.

RTMs activated with **M-CSF** became larger and rounded up, as both the whole area as well as the fixed and mobile area increased, while the perimeter stayed in the range of the control cells (S2 Fig). The trend of cell area and perimeter as well as the trend of the aspect ratio were also increased, indicating that RTMs could continue to grow during and after our observation period (S2 Fig). Because M-CSF generally

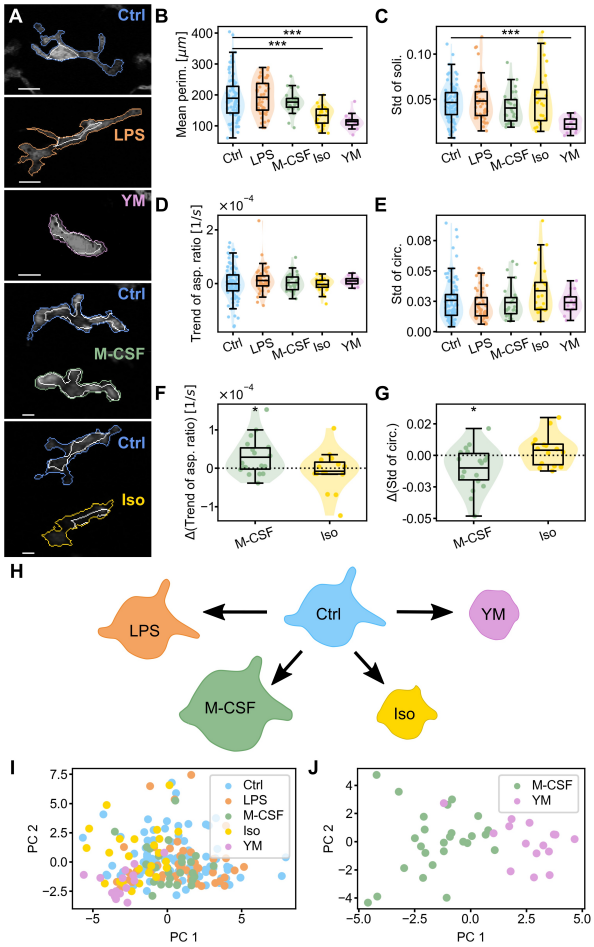

Fig 3. Comparison of RTMs *in vivo* subjected to different chemical stimulations. (A) Snapshots of RTMs under different conditions: Control (Ctrl), Lipopolysaccharides (LPS), Macrophage Colony Stimulating Factor (M-CSF), an overdose of Isoflurane (Iso) and YM201636 (YM). For M-CSF and Isoflurane, the (same) cells were first imaged under Ctrl conditions (top), then after stimulus was applied (bottom). The cell perimeter (colored) and the outline of its fixed area (white) are marked; the length of all scale bars is 10 µm. (B-G) Comparison of the different chemical conditions using selected cell size and shape features. The mean of the population is marked, tests for statistical significance were performed using a two-sided permutation t-test for whole population comparison (B-E) and a one-sided t-test for direct comparisons of identical cells (F, G). Here, for each cell/ cell pair, the parameter of the control cell was subtracted from the parameter of the cell under perturbation. Significance is abbreviated as * $p \leq 0.05$, ** $p \leq 0.01$, *** $p \leq 0.001$. (B) Mean cell perimeter. (C) Standard deviation of cell solidity. (D) Trend of cell aspect ratio. (E) Standard deviation of circularity. (F) Trend of aspect ratio, comparing identical cells. (G) Standard deviation of circularity, comparing identical cells. (H) Sketch showing (strongly exaggerated) the qualitative changes in RTM morphology for the different chemical stimuli. (I) Principal component analysis of all 20 cell parameters for the five conditions. (J) Principal component analysis of all 20 cell parameters comparing only the M-CSF and the YM-201636 cell populations.

increases the endocytotic activity and phagocytic capabilities of RTMs, we found that the size of RTMs also increased which would be consistent with the higher uptake.

RTMs which responded to a shut-down of systemic circulation due to the overdose of the sedative **Isoflurane** shrank and rounded up as well as decreased their sampling activities. The shrinking of the cell was demonstrated by a decreased mean cell perimeter and whole and mobile area, while the fixed area of the cells increased as compared to control conditions (see Fig 3 B and S2 Fig). The rounding up of cells could be seen via the increased solidity, convexity and circularity of the cells, which would increase even further as indicated by an increased trend of solidity and circularity (see S3 Fig). A decreased standard deviation of the cell perimeter (S2 Fig) as well as of the aspect ratio (S3 Fig) supported the suspended sampling activities and thus reduced dynamic state of the RTMs.

With **YM201636**, it was visually apparent that the cells became rounder, swelling, and less active. This observation was confirmed by our cell morphology parameters where the rounder cell shape could be detected via the decreased mean cell perimeter (Fig 3 B) and increased mean cell solidity, circularity and convexity (S3 Fig). The swelling aspect was supported by the increased fixed area with a decreased mean whole and mobile area (S2 Fig) at the same time, hinting that the cell volume expands into the third dimension (orthogonal to the projection plane of the images) not shown in our 2D representation. The lower dynamic activity of the cells was revealed by the significantly decreased standard deviation of cell perimeter, area, solidity, convexity and aspect ratio (see S2 Fig and S3 Fig). This is consistent with the expectation that cells under the influence of YM201636 were unable to dissolve endosomes within their cell body, and thus failed to mobilize additional membranes to form sampling protrusions. The qualitative changes in RTM morphology under the different conditions are summarized in Fig 3 H.

Here, we were able to use our rather large set of quantifiers to interpret and thus verify the qualitative cell morphological changes of RTMs under controlled perturbations. Next, we aim to facilitate classification of cells of different conditions by means of dimensionality reduction of the large set of quantifiers given.

Dimensionality reduction methods for morphology quantifiers show large heterogeneity of unperturbed RTM shape and dynamics

While having many different cell morphology parameters is advantageous to define changes in cell appearances, summarizing the parameters by dimensionality reduction tools will be useful to identify parameters that best differentiate morphologies of RTMs under the different conditions. In addition, a reduced dimensionality space can be used to assign cells in an unknown state to a specific condition or functional state based on the cell morphology and dynamics alone.

Interestingly, for the given features and the given conditions, a clear clustering of every single cell population could not be achieved in the Principal Component Analysis (PCA) (Fig 3 I). Other approaches of dimensionality reduction including both linear and non-linear methods, such as t-SNE or UMAP, were tested additionally, but did not lead to significantly different results of discriminating between the cell populations (S5 Fig, A-E). However, it was evident that cells treated with YM201636 clustered together, and cells treated with Isoflurane also showed a clear trend in the PCA.

We argue that the reason for the lack of clustering for the sub-populations corresponding to other conditions may lie in the very broad distribution of the cells of the control population in the parameter space, which can also be seen in Fig 3 B-E, S2 Fig A-H and S3 Fig A-L. This broad distribution - representing a large heterogeneity of

the morphology and dynamics of cells in steady state - was also visible in other dimensionality reduction methods and thus seemed to be a general feature, independent of the reduction method. Furthermore, we checked that the cells coming from the same experiment are sufficiently dispersed in the PCA representation, indicating that this dispersal of the morphology of the control cell population was not due to varying experimental conditions of the different experiments (see S5 Fig F).

We speculated that while the control condition embraces cells with broadly varying shape and shape dynamics properties, chemical perturbations narrow down the respective distribution. Indeed, using PCA to compare the effect of the two chemical stimuli that should result in opposite cell morphologies - here M-CSF being a 'positive', activating stimulus and YM201636 which in principle shuts down all cell dynamics - provided two clear and distinct cell populations (Fig 3 J).

One of the advantages of using PCA analysis is the ability to easily link principal components to the original parameters. Interestingly, for both considered PCAs (including either all conditions or only M-CSF or YM-treated RTMs), the structure of the principal components (PC) was rather similar: PC1 was mostly comprised of static parameters like the mean perimeter or mean circularity or the RTMs, whereas the main features contributing to PC2 were the trends of, for example, perimeter or convexity thus including information about the development and dynamics of the measured parameters.

In summary, we found that the population of RTMs in the steady state is characterized by a very broad distribution of cell shape and dynamics, whereas chemical perturbation of the cell state constrains the morphodynamical phenotype that the RTMs can show. We next sought to use the same quantification factors in a new physiological context, namely to establish a practical explant platform of the peritoneal serosa to study morphology and dynamics of RTMs *in situ* but independent of the living organism.

Improving tissue explant viability by monitoring RTM morphology and dynamics

Intravital imaging is crucial for biomedical research to understand immunological processes in living organisms. However, the technique is involved and image quality can be easily compromised by numerous internal and external influences and therefore more accessible and practical alternatives are needed. Many constraints and parameters could be better controlled by explanting the tissue compartment, thereby making the approach more experimentally versatile. However, it is critical to ensure that the conditions to which the cells are exposed in the process are as close as possible to *in vivo* imaging. Our shape analysis pipeline is an ideal instrument to monitor and verify that cell shapes and dynamics are comparable under explant and intravital imaging conditions.

To investigate this possibility, mouse peritoneal tissue was explanted with the abdominal wall, transferred to a tissue culture system, and the cells were imaged immediately thereafter (Expl direct), see Materials and Methods. Our shape analysis showed that those explanted RTMs have an overall smaller cell size, as visible considering the cell perimeter, area and mobile area (Fig 4 B, S4 Fig A-C), whereas the mean cell shape was rarely affected by their new environmental conditions (Fig 4 C, S4 Fig I-L). However, the standard deviation of almost every single feature was decreased (S4 Fig E, F, M-P), see for example the standard deviation of solidity (Fig 4 D). Therefore, the RTMs in the explanted tissue seemed to be less active and have decreased their sampling activity. Interestingly, the trend of almost every feature - which shows long-term evolution in the time series of the quantifiers - was significantly different for the RTMs which were directly imaged after explantation compared to the

cells imaged *in vivo*. These observations suggest that the RTMs in the explanted tissue needed time to adapt to their new culture environment.

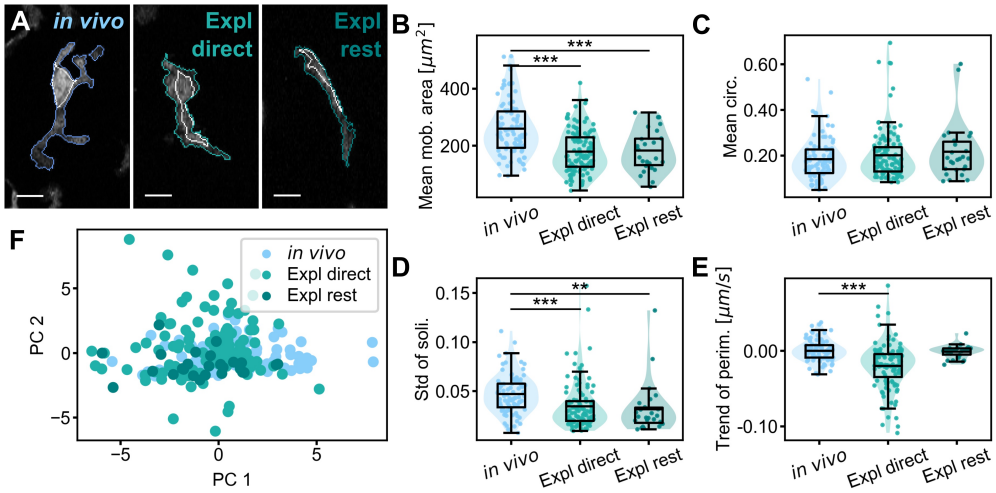

Fig 4. Comparison of RTMs *in vivo* to explanted RTMs. (A) Snapshots of RTMs with different experimental setups. Peritoneal macrophages imaged *in vivo* serve as the control population. The tissue was explanted and the cells either were imaged immediately after (Expl direct) or were given time to rest and adjust to the new 'environment' in an imaging chamber for 1 hour (Expl rest). Scale bar amounts to 10 µm. (B-E) Comparison of the different chemical conditions using selected cell size and shape parameters. The mean of the population is marked, tests for statistical significance were performed using a two-sided permutation t-test for population comparison. Significance is abbreviated as * $p \leq 0.05$, ** $p \leq 0.01$, *** $p \leq 0.001$. (B) Mean of cell perimeter. (C) Standard deviation of cell solidity. (D) Mean cell circularity. (E) Trend of cell aspect ratio. (F) Principal component analysis (PCA) of all cell size and shape parameters for the three cell populations.

To test this hypothesis, we allowed the explanted tissue to rest in the culture system for one hour (Expl rest) and then repeated our measurements. Similar to the explanted cells imaged directly, cell shape was again comparable to RTMs *in vivo*, whereas both cell size (Fig 4 B, S4 Fig A-C) and cell dynamics were reduced (S4 Fig E, F, M-P). However, the trends of our quantifiers for explanted cells imaged after 1 hour were comparable to those of control cells *in vivo*, indicating that RTMs indeed had to adapt to their new environment after explantation.

Next, we performed a PCA using all available cell morphology parameters to see if the three cell populations could be distinguished from each other. Although we found significant differences in cell shape and size between RTMs in different environments, the three populations appeared to be highly heterogeneous and scattered in the PCA (Fig 4 F). To verify that this heterogeneity is not due to variability in individual experiments, we color-coded cells from the same experiments in the PCA map. Here, we found that cells from the individual experiments did not cluster together, but instead scattered, supporting the conclusion that the observed heterogeneity in cell morphologies was indeed due to the underlying tissue itself (S6 Fig F). This heterogeneity of morphologies in explanted cells was also evident when using other dimensionality reduction methods, like t-SNE or UMAP, which are shown in S6 Fig A-E.

Taken together, the explantation method with an additional resting time essentially preserved the RTM forms compared to cells *in vivo*. Also the large heterogeneity of cell morphology and dynamics as visible in the PCA was retained for the cells of the

explanted tissues. However, the size of the RTMs as well as their dynamics, as measured by the standard deviation of the quantifiers, was still smaller compared to cells *in vivo*. Therefore, it was obvious that a better apparatus setup and optimized culture conditions are still needed to better match the sampling activity of the RTMs to the dynamics *in vivo*.

Discussion

In this paper, we employed an intravital imaging technique with high spatial and temporal resolution to visualize sampling dynamics of RTMs under resting conditions and in response to various chemical and physiological perturbations. We analyzed the cell morphology and dynamics with a custom-built image processing pipeline with a set of cell size and shape parameters, by which we could quantitatively assess the influence of chemical stimuli on cell dynamics and morphology of RTMs. We demonstrated that the parameters of this pipeline quantify the qualitative behavior and morphological changes of an RTM over time in a human-interpretable way. We then used the set of quantifiers to differentiate cells in various functional states - e.g., upon "shut down" of the host organism - from their equilibrium resting state. The qualitative morphology changes associated with these functional states could be inferred directly from the quantitative measurements. Finally we have used the cell morphology features to monitor the health of RTMs in an explanted tissue fragment and could suggest the improvement of the experimental protocol.

Our analysis pipeline is based on the assumption that the individual cells can be adequately segmented as instances over time so that their morphology and dynamics can then be measured quantitatively. In this study, segmentation is facilitated by using 2D images instead of the actual 3D data, since most of the dynamics occur along the x- and y-axis of the imaging plane. Despite the loss of third dimension information, we could not measure an obvious long-term trend of the individual features of cell morphology over time, indicating the conservation of volume that the RTMs must obey. As every segmentation procedure, also our implementation for the case of the RTMs has limitations. Some cells had to be excluded from being analyzed, because parts of their cell body - mostly protrusions - were not always detected reliably over time. That also means that the image segmentation is not yet fully automated as the segmentation needs to be manually adjusted and several thresholds - e.g. which portions of the cell area should be considered as fixed area - were also estimated, but not computationally optimized. Emerging machine- or deep-learning applications like ilastik [24] or Cellpose [25], may in future improve reliable detection of the whole RTM cell body when sufficiently trained. In that case, our pipeline can easily be applied to new segmentation results. Since sampling surveillance can be considered a core function of all macrophages *in vivo*, it would be highly interesting to use the established image processing and analysis pipeline also on RTMs in other tissue niches and organs. However, we still lack similar experimental approaches to study the morphodynamics of macrophages in other peripheral tissues with a comparable spatial and temporal resolution and experimental versatility as provided by our peritoneal platform. Just as the transcriptional phenotype of macrophages is dictated by the stromal environment, the tissue itself can have an impact on the morphodynamics of macrophages. Anatomical constraints and physical barriers are not currently taken into account in our modeling approach. Further visualization tools are needed for this - because "the dark is (almost) never empty".

We demonstrated that the dynamic behavior of RTMs in the submesothelial peritoneum is non-uniform at steady state. Although RTM heterogeneity is a product of various intrinsic (e.g. ontogenesis) and extrinsic (e.g. niche imprinting) factors, it is nevertheless remarkable that this putatively homogeneous population of RTMs [6]

exhibits a high degree of morphodynamic variation within a confined tissue compartment with respect to different shape descriptors and across different experiments. One possible reason for this could be that the presence of many different cell morphologies and thus dynamic phenotypes within a tissue means that the system is better prepared to respond quickly to acute stress stimuli. Such intrinsic variability allows for greater adaptive plasticity of the tissue as a whole and thus a more dynamic adaptation to acutely changing external conditions. Another interesting possibility for the heterogeneity within the quiescent population is that RTMs must cycle their activities over time. Due to the large amounts of extracellular fluids they take up during active sampling, there could be a certain time when RTMs need to "digest" everything they have internalized - and during this time their uptake activity could be diminished, leading to a more passive dynamic behavior. Whether uptake and digestion can occur simultaneously *in vivo* or require such a cyclic sampling behavior needs to be investigated by further in-depth cellular studies.

The repertoire of quantifiers of RTM shape and dynamics can still be extended: One can analyze the cell outline by measuring its curvature, as has been previously done for the shape of arteries [28]. By determining the displacement of the cell contour to find active and inactive areas of the cell membrane during the dynamics of the sampling process, the dynamic behavior of the individual protrusions themselves and their movement pattern can then be specifically assessed. To better understand the temporal dimension of the sampling behavior, the different quantifiers need to be integrated over time, for example by calculating the Fourier transform to reveal a possible periodicity or the autocorrelation function to identify possible characteristic time scales. An oscillatory behavior or pattern (as already partially visible in Fig 2 C, D) may then emerge, providing insights into the mechanisms of the sampling behavior of the RTMs at cellular or the tissue-level. Finally, with more parameters to choose from, it might be possible to use PCA (as in Fig 3 I) to group the cells from different conditions and automatically classify a RTM and its activation status. Conversely, we might also find even more clues about how heterogeneous and diverse cells within a given tissue niche actually are.

Quantifying the morphology and dynamics of RTMs has helped us to assess the state of macrophages when exposed to different pathological and physiological conditions, even when the tissue has been explanted. While the shape of the RTMs was preserved in the explantation method used, we have learned that there is more to a functionally healthy tissue than the mere passive presence of cells. We recognize their cellular morphodynamics as an important expression of a physiological tissue state. We found that while the cells need time to adapt to their new environment before they are imaged, they are still smaller and less active compared to RTMs *in vivo*. To better understand the biology of RTMs, new experimental platforms are needed, such as organ-on-a-chip approaches or tissue explants. Our modular analysis pipeline now enables scientists to quantitatively test new explantation techniques, tissue culture systems and platform designs to determine how similar the explanted RTMs perform morphodynamically to their *in vivo* counterpaarts.

Materials and methods

Intravital imaging of the peritoneal serosa

For intravital microscopy of the peritoneal serosa LysM-Cre x tdTom F1 animals between 10 to 18 weeks have been used to allow the visualization of peritoneal macrophages. Intravital imaging was done as previously [6] described with slight modifications. Imaging was performed on a Zeiss LSM 880 NLO two photon microscope equipped with a 20x water immersion objective (Zeiss; W PlanApochromat 20x/1,0

DIC D=0,17 M27 75mm, Cat#421452-9880-000). Animals were anesthetized with isoflurane (cp pharma; Cat#1214). The animal was shaved and a midline incision was made into the abdominal wall. Subsequently, another incision into the peritoneal wall was made along the linea alba to expose the peritoneal serosa. The peritoneal wall was carefully retained using two small sutures (Ethicon; coated VICRYL-polyglactin 6/0; Cat#V134H) and mounted on a 12 × 25 mm plastic base plate with a raised 12 mm circular plate using Vetbond (3M; Cat#1469SB). 10 µL of sterile pre-warmed HBSS buffer with Ca+ and Mg+ (Gibco; Cat#14025-050), containing MCSF or LPS, was applied onto the surface, before covering the serosa with a sterilized cover glass (Paul Marienfeld; Cat#4663433). The animal was then transferred to the heated microscopic imaging chamber. The serosa was kept at a temperature of 36 °C using an adjustable heater (WPI; Air-Therm SMT). For some animals control baseline recording was performed before adding the respective stimuli (M-CSF). Animals which showed signs of surgical damage or bleeding were not studied further. Data were acquired at a resolution of 512 × 512 (12 bit) in stacks of 12 frames each 3 µm apart at a frame rate of 943.72 ms and a zoom of 1.5 using ZEN software (Zen 2.1 SP3; Zeiss). For imaging, the laser was tuned to 930 nm and the following filter cubes were used: (SP 485; BP 500-550; BP 575-610). Raw imaging data were processed and analyzed with Imaris 9.5.1 (Bitplane).

Administration of chemical stimuli

Chemical stimuli like M-CSF and LPS were directly added to 10 µL of sterile pre-warmed HBSS buffer with Ca+ and Mg+ (Gibco; Cat#14025-050), which was applied onto the peritoneal serosa surface, before covering the serosa with a sterilized cover glass (Paul Marienfeld; Cat#4663433). For details about the administration of YM201636, please refer to [5]. For experiments using the same animal before and after the stimuli, baseline recordings were performed just using HBSS buffer as control. After recording the baseline, the coverslip was slightly lifted and M-CSF was carefully added to the buffer without changing the animals position.

Explantation and imaging of the explanted peritoneal serosa

For the explanted peritoneal serosa animals were prepared in a similar way as for the intravital imaging of the serosa. Animals were sacrificed, shaved and a midline laparotomy performed. A chalazion forceps was carefully inserted into the abdomen without touching the peritoneal serosa. After tightening the forceps, holding the serosa in place, scissors were used to cut around the forceps. The tissue was immediately transferred to a petri dish filled with prewarmed cell culture media (50% FCS, 25% HBSS, 24% MEM, 1% P/S) and transferred to the imaging chamber. Imaging parameters were kept the same as for the *in vivo* imaging.

Image segmentation and labeling

The 3D images were converted to 2D by using a maximum intensity projection in Fiji [29], then all further processing and extraction steps were performed in Python.

First, the 2D grayscale image (Fig 5 A) was segmented with the RTMs as foreground using an adaptive threshold via Li's iterative Minimum Cross Entropy Method [30] as implemented in [31]. In a further preprocessing step before labeling the cells, the objects (i.e. cells) of the resulting binary image (Fig 5 B) were smoothed using binary opening as implemented in the scikit-image package [31] with a circular structuring element of radius 0.6 µm. In the following step, small holes in the cells smaller than 10 µm and small objects in the background smaller than 10 µm were removed, resulting in the smoothed binary image as shown in Fig 5 C.

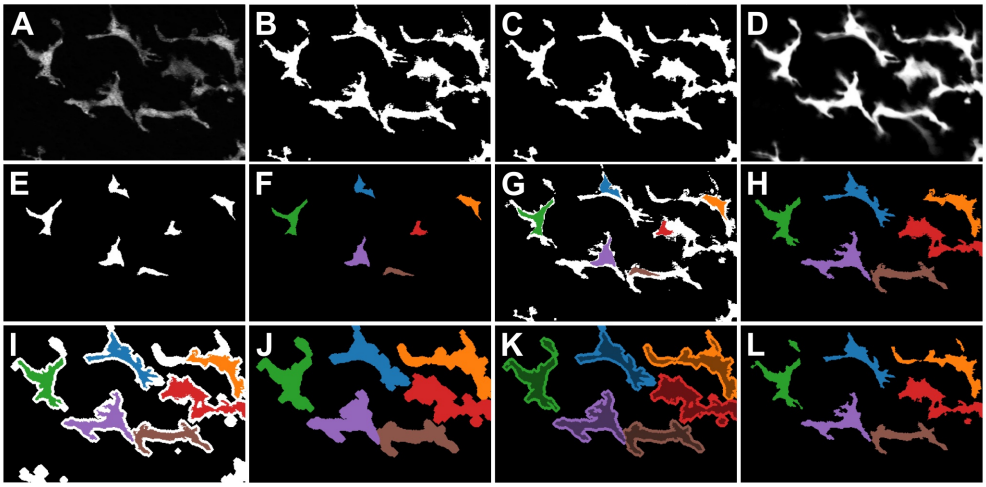

Fig 5. Visualization of the image segmentation and labeling pipeline for the first frame of an example movie. (A) Grayscale image. (B) Binarized image obtained (from (A)) using thesholding via Li's iterative Minimum Cross Entropy Method. (C) Smoothed binarized image. (D) Integrated movie over all time frames. (E) Integrated movie with fixed area using a thershold of 0.97 on (D). (F) Label seeds obtained from (E) by coloring all distinct objects. (G) Overlay of label seeds and binary segmented cells. (H) Labeling all distinct objects to be used as seed labels. (G) Overlay of (B) and (F), using watershed algorithm to label the cells according to the seed values resulting in (H). (I) Dilating the cells from (B) and using the labeled cells from (H) as seed labels for the watershed algorithm to achieve the labeling as shown in (J). (K) Using the labels from (J) to correctly label the pre-processed binary images from (C). (L) Final labelled image.

In order to label the cells individually the watershed algorithm - implemented in scikit-image [31] - was used which requires a set of seed labels. These seed labels were generated by applying a threshold of 0.97 to the mean of the movie over time (Fig 5 E, F), removing any objects that are smaller than 50 µm and then assigning individual labels to the remaining distinct objects (Fig 5 G). Using these labeled objects as input for the watershed algorithm to label the cells from Fig 5 B, a preliminary labeled image was obtained as shown in Fig 5 H. Here, protrusions that were disconnected in the binarization process were not labeled as belonging to the cells, as seen for example for the green or orange cell. In order to correct for that, the binary image from Fig 5 B was dilated using a diamond-shaped structuring element with a radius of 2.2 µm and the preliminary labeled image (Fig 5 H) was used as seed labels for the watershed algorithm (Fig 5 I, J). Finally, the resulting labeled and dilated cells are used as overlay for the smoothed binary image (Fig 5 K) and the final labeled image is obtained (Fig 5 L). As visible in Fig 5 L, some labeled objects such as the red colored mass are actually composed of two cells. Therefore, the labeled movies were individually examined and compared to the 3D images to verify which of the labeled objects are actually individual and whole macrophages. In this step, there were also macrophages identified that were labeled as two distinct objects, which was corrected by merging the initial seed labels that wrongfully had two different labels for one single cell. The number of RTMs labeled correctly itemized by the different conditions using the just described method is summarized in Table 1.

Table 1. Summary of the extracted amounts of RTMs using the labeling pipeline on the available data.

Condition	Ctrl	LPS	M-CSF	Iso	YM	Expl direct	Expl rest
Amount of experiments	18	12	5	2	1	12	3
Amount of labeled objects	164	86	48	37	25	217	49
Amount of correctly labeled RTMs	92	49	26	24	15	119	26

Supporting information

S1 Fig. Mean image intensity over time for the cell visualised in Fig 2.

S2 Fig. Comparing different chemically induced activations *in vivo* using cell size quantifiers. (A) Mean of cell perimeter. (B) Mean of cell area. (C) Mean of mobile cell area. (D) Fixed cell area. (E) Standard deviation of cell perimeter. (F) Standard deviation of cell area. (G) Slope of a linear fit to cell perimeter. (H) Slope of a linear fit to cell area. (I - P) Direct comparison of the same cells first under Control, then under chemically induced conditions. The parameter value of the Ctrl condition was subtracted from the parameter value under chemical condition. (I) Mean of cell perimeter. (J) Mean of cell area. (K) Mean of mobile cell area. (L) Fixed cell area. (M) Standard deviation of cell perimeter. (N) Standard deviation of cell area. (O) Slope of a linear fit to cell perimeter. (P) Slope of a linear fit to cell area. Significance is abbreviated as * $p \leq 0.05$, ** $p \leq 0.01$, *** $p \leq 0.001$.

S3 Fig. Comparing different chemically induced activations *in vivo* using cell shape quantifiers. (A) Mean of solidity. (B) Mean of convexity. (C) Mean of circularity. (D) Mean of aspect ratio. (E) Standard deviation of solidity. (F) Standard deviation of convexity. (G) Standard deviation of circularity. (H) Standard deviation of aspect ratio. (I) Slope of a linear fit to solidity. (J) Slope of a linear fit to convexity. (K) Slope of a linear fit to circularity. (L) Slope of a linear fit to aspect ratio.

(M - X) Direct comparison of the same cells first under Control, then under chemically induced conditions. The parameter value of the Ctrl condition was subtracted from the parameter value under chemical condition. (M) Mean of solidity. (N) Mean of convexity. (O) Mean pf circularity. (P) Mean of aspect ratio. (Q) Standard deviation of solidity. (R) Standard deviation of convexity. (S) Standard deviation of circularity. (T) Standard deviation of aspect ratio. (U) Slope of a linear fit to solidity. (V) Slope of a linear fit to convexity. (W) Slope of a linear fit to circularity. (X) Slope of a linear fit to aspect ratio. Significance is abbreviated as * $p \leq 0.05$, ** $p \leq 0.01$, *** $p \leq 0.001$.

S4 Fig. Comparing different tissue preparation techniques using cell size and shape quantifiers. The cells imaged *in vivo* serve as control, explanted cells were either imaged directly after explantation (Expl direct), or they were given 1 hour in an imaging chamber to rest and adapt to their new environment (Expl rest). (A) Mean of cell perimeter. (B) Mean of cell area. (C) Mean of mobile area. (D) Fixed area. (E) Standard deviation of cell perimeter. (F) Standard deviation of cell area. (G) Slope of a linear fit to the cell perimeter. (H) Slope of a linear fit to the cell area. (I) Mean of solidity. (J) Mean of convexity. (K) Mean of circularity. (L) Mean of aspect ratio. (M) Standard deviation of solidity. (N) Standard deviation of convexity. (O) Standard deviation of circularity. (P) Standard deviation of aspect ratio. (Q) Slope of a linear fit to solidity. (R) Slope of a linear fit to convexity. (S) Slope of a linear fit to circularity. (T) Slope of a linear fit to aspect ratio. Significance is abbreviated as * $p \leq 0.05$, ** $p \leq 0.01$, *** $p \leq 0.001$.

S5 Fig. Comparing different dimensionality reduction methods for differently chemically activated RTM cell populations. (A) - (E): Colors are blue for Control, orange for LPS, green for M-CSF, yellow for Isoflurane, pink for YM201636. (A) Linear Discriminant Analysis. (B) Neighborhood Components Analysis. (C) Locally Linear Embedding. (D) T-distributed Stochastic Neighbor Embedding. (E) Uniform Manifold Approximation and Projection. (F) Principal Components Analysis, where all chemically activated cell populations are marked as stars and the control cell population is colored according to their corresponding experiment.

S6 Fig. Comparing different dimensionality reduction methods for cell populations in differently prepared tissues. (A) - (E): Colors are blue for *in vivo* control, seagreen/ light greenish for Explant direct, teal/ dark greenish for Explant rested for 1 hour before imaging. (A) Linear Discriminant Analysis. (B) Neighborhood Components Analysis. (C) Locally Linear Embedding. (D) T-distributed Stochastic Neighbor Embedding. (E) Uniform Manifold Approximation and Projection. (F) Principal Components Analysis, where the *in vivo* cell population and the rested Explant cell populations are marked as stars and the explanted and directly imaged cell population is colored according to their corresponding experiment.

S1 Video. BMDMs migrating *in vitro*. Video showing migrating BMDMs in a culture dish, corresponding to the snapshots in Fig 1.

S2 Video. RTMs sampling *in vivo*. Video showing sampling RTMs in the peritoneal serosa, corresponding to the snapshots in Fig 1.

S3 Video. RTM *in vivo* with measured features animated. Video showing sampling RTM *in vivo* together with the measured features, corresponding to the snapshots in Fig 1.

S1 Table. Values for boxplots from S2 Fig, S3 Fig, S4 Fig. The mean (M), standard deviation (SD) and p-value (p) of the single cell morphodynamics quantifier are given - however, the latter is only given if the mean of a certain condition was significantly different from the control condition, i.e., $p \leq 0.05$.

Acknowledgments

MS acknowledges the ongoing support from the graduate school IMPRS Physics and Medicine throughout her research. SU is supported by the DFG (project-IDs 448121430, 405969122, 447268119), the Hightech Agenda Bavaria and by an ERC starting grant (project-ID 101039438). Dynamic imaging was performed on a DFG-funded confocal microscope (project-ID 261193037) and a DFG-funded spinning disc microscope (248122450). VZ acknowledges the support by the DFG (German Research Foundation); project A7 within the Research Training Group “Immunomicrotope” (GRK 2740/447268119).

References

1. Sender R, Weiss Y, Navon Y, Milo I, Azulay N, Keren L, et al. The total mass, number, and distribution of immune cells in the human body. Proc Natl Acad Sci. 2023 Oct;120(44):e2308511120.

2. Nobs SP, Kopf M. Tissue-resident macrophages: guardians of organ homeostasis. Trends Immunol. 2021 Jun;42(6):495–507.

3. Okabe Y, Medzhitov R. Tissue biology perspective on macrophages. Nat Immunol. 2016;17(1):9–17.

4. Mass E, Nimmerjahn F, Kierdorf K, Schlitzer A. Tissue-specific macrophages: how they develop and choreograph tissue biology. Nat Rev Immunol. 2023 Mar;23:563–579.

5. Freeman SA, Uderhardt S, Saric A, Collins RF, Buckley CM, Mylvaganam S, et al. Lipid-gated monovalent ion fluxes regulate endocytic traffic and support immune surveillance. Science. 2020 Jan;367:301–305

6. Uderhardt S, Martins AJ, Tsang JS, Lämmermann T, Germain RN. Resident Macrophages Cloak Tissue Microlesions to Prevent Neutrophil-Driven Inflammatory Damage. Cell. 2019;177(3):541-555.e17.

7. Ipseiz N, Uderhardt S, Scholtysek C, Steffen M, Schabbauer G, Bozec A, et al. The Nuclear Receptor Nr4a1 Mediates Anti-Inflammatory Effects of Apoptotic Cells. J Immunol. 2014 May;192(10):4852–8.

8. Bodor DL, Pönisch W, Endres RG, Paluch EK. Of Cell Shapes and Motion: The Physical Basis of Animal Cell Migration. Dev Cell. 2020 Mar;52(5):550–62.

9. Yevick HG, Martin AC. Quantitative analysis of cell shape and the cytoskeleton in developmental biology. WIREs Dev Biol. 2018 Nov;7(6):e333.

10. Boquet-Pujadas A, Olivo-Marin JC, Guillén N. Bioimage Analysis and Cell Motility. Patterns. 2021 Jan;2(1):100170.

11. Prasad A, Alizadeh E. Cell Form and Function: Interpreting and Controlling the Shape of Adherent Cells. Trends Biotechnol. 2019 Apr;37(4):347–57.

12. Pincus Z, Theriot JA. Comparison of quantitative methods for cell-shape analysis. J Microsc. 2007;227(2):140–56.

13. Mingqiang Y, Kidiyo K, Joseph R. A Survey of Shape Feature Extraction Techniques. Pattern Recognition Techniques, Technology and Applications. InTech; 2008

14. Radojević M, Smal I, Meijering E. Automated neuron morphology reconstruction using fuzzy-logic detection and Bayesian tracing algorithms. In: 2015 IEEE 12th International Symposium on Biomedical Imaging (ISBI). 2015. p. 885–8

15. Tweedy L, Meier B, Stephan J, Heinrich D, Endres RG. Distinct cell shapes determine accurate chemotaxis. Sci Rep. 2013 Sep;3(1):2606

16. Zanier ER, Fumagalli S, Perego C, Pischiutta F, De Simoni MG. Shape descriptors of the “never resting” microglia in three different acute brain injury models in mice. Intensive Care Med Exp. 2015 Feb 24;3(1):7.

17. McWhorter FY, Wang T, Nguyen P, Chung T, Liu WF. Modulation of macrophage phenotype by cell shape. Proc Natl Acad Sci. 2013 Oct 22;110(43):17253–8.

18. Hu G, Su Y, Kang BH, Fan Z, Dong T, Brown DR, el al. High-throughput phenotypic screen and transcriptional analysis identify new compounds and targets for macrophage reprogramming. Nat Commun. 2021 Feb 3;12(1):773.

19. Bode JG, Ehlting C, Häussinger D. The macrophage response towards LPS and its control through the p38MAPK–STAT3 axis. Cell Signal. 2012 Jun;24(6):1185–94.

20. Nemunaitis J. Macrophage function activating cytokines: potential clinical application. Crit Rev Oncol Hematol. 1993 Apr;14(2):153–71.

21. Jefferies HBJ, Cooke FT, Jat P, Boucheron C, Koizumi T, Hayakawa M, et al. A selective PIKfyve inhibitor blocks PtdIns(3,5)P 2 production and disrupts endomembrane transport and retroviral budding. EMBO Rep. 2008 Feb;9(2):164–70.

22. Williams LM, Ridley AJ. Lipopolysaccharide Induces Actin Reorganization and Tyrosine Phosphorylation of Pyk2 and Paxillin in Monocytes and Macrophages. J Immunol. 2000 Feb 15;164(4):2028–36.

23. Pi J, Li T, Liu J, Su X, Wang R, Yang F, et al. Detection of lipopolysaccharide induced inflammatory responses in RAW264.7 macrophages using atomic force microscope. Micron. 2014 Oct;65:1–9.

24. Berg S, Kutra D, Kroeger T, Straehle CN, Kausler BX, Haubold C, et al. ilastik: interactive machine learning for (bio)image analysis. Nat Methods. 2019 Dec;16(12):1226–32.

25. Stringer C, Wang T, Michaelos M, Pachitariu M. Cellpose: a generalist algorithm for cellular segmentation. Nat Methods. 2021 Jan;18(1):100–6.

26. Blériot C, Chakarov S, Ginhoux F. Determinants of Resident Tissue Macrophage Identity and Function. Immunity. 2020 Jun 16;52(6):957–70.

27. Jenkins SJ, Allen JE. The expanding world of tissue-resident macrophages. Eur J Immunol. 2021;51(8):1882–96.

28. Onkaew D, Turior R, Uyyanonvara B, Akinori N, Sinthanayothin C. Automatic retinal vessel tortuosity measurement using curvature of improved chain code. In: International Conference on Electrical, Control and Computer Engineering 2011 (InECCE) 2011;183–6.

29. Schindelin J, Arganda-Carreras I, Frise E, Kaynig V, Longair M, Pietzsch T, et al. Fiji: an open-source platform for biological-image analysis. Nat Methods. 2012 Jul;9(7):676–82.

30. Li CH, Lee CK. MINIMUM CROSS ENTROPY THRESHOLDING. Pattern Recognit. 1993;26:9.

31. van der Walt S, Schönberger JL, Nunez-Iglesias J, Boulogne F, Warner JD, Yager N, et al. scikit-image: image processing in Python. PeerJ. 2014 Jun 19;2:e453.

32. Pedregosa F, Varoquaux G, Gramfort A, Michel V, Thirion B, Grisel O, et al. Scikit-learn: Machine Learning in Python. J Mach Learn Res. 2011;12(85):2825–30.

33. Efron B, Hastie T. Computer Age Statistical Inference. Cambridge University Press; 2016.

34. Virtanen P, Gommers R, Oliphant TE, Haberland M, Reddy T, Cournapeau D, et al. SciPy 1.0: fundamental algorithms for scientific computing in Python. Nat Methods. 2020 Mar;17(3):261–72.

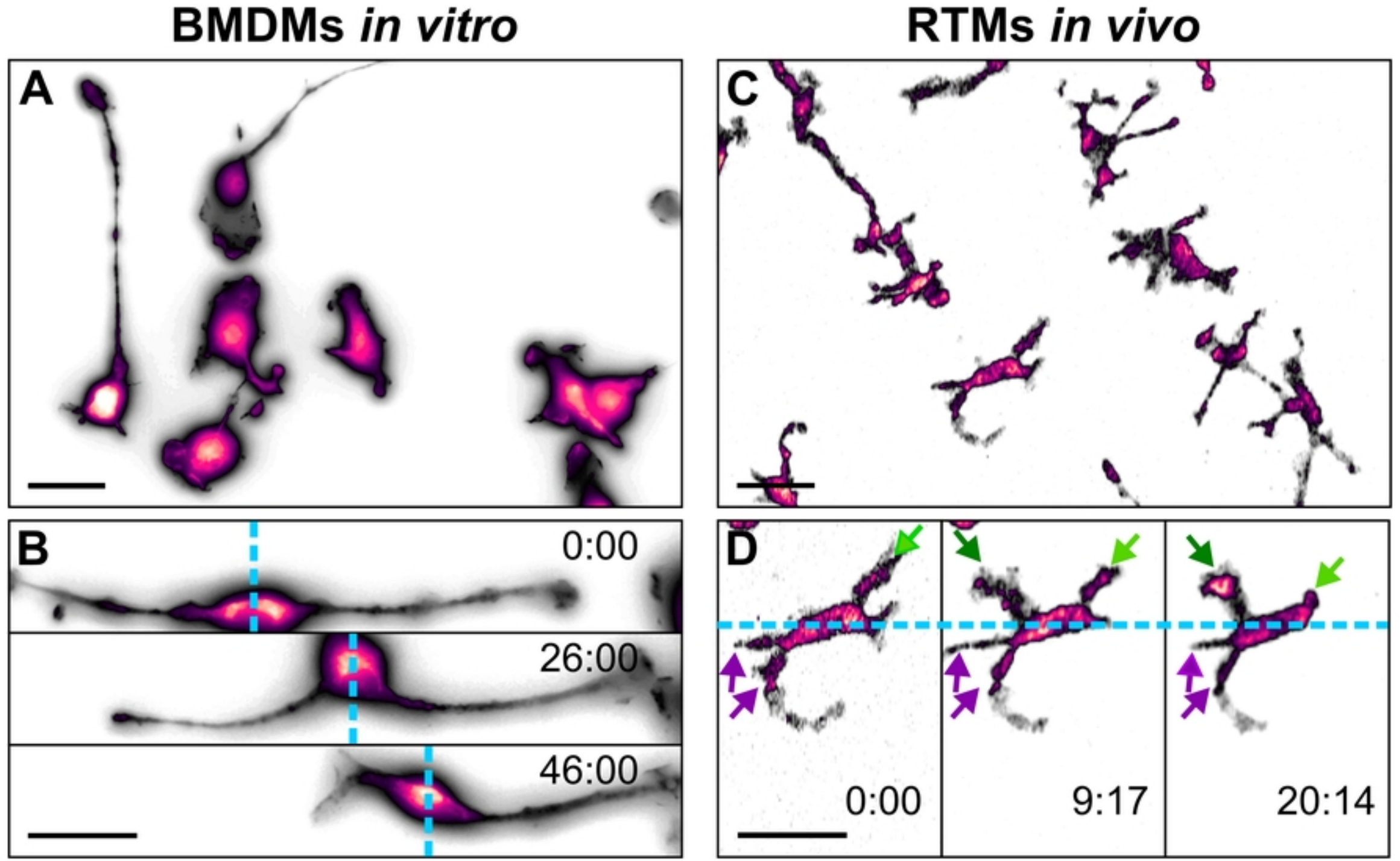

Figure 1

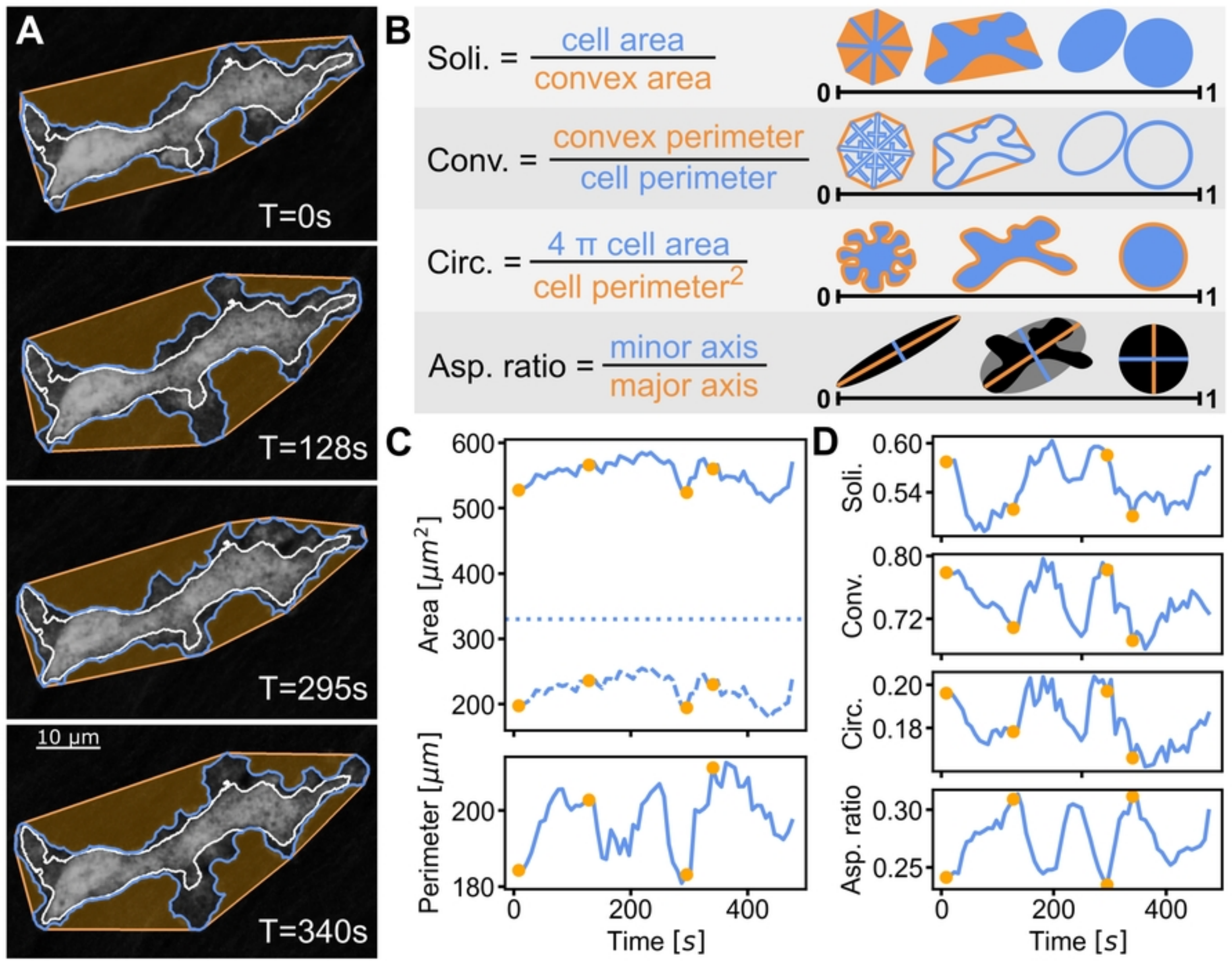
A
T=0s
T=128s
T=295s
10 µm
T=340s
B
Soli. = cell area / convex area
Conv. = convex perimeter / cell perimeter
Circ. = 4 π cell area / cell perimeter²
Asp. ratio = minor axis / major axis
0
1
C
Area [µm²]
Perimeter [µm]
Time [s]
D
Soli.
Conv.
Circ.
Asp. ratio
Time [s]

Figure 2

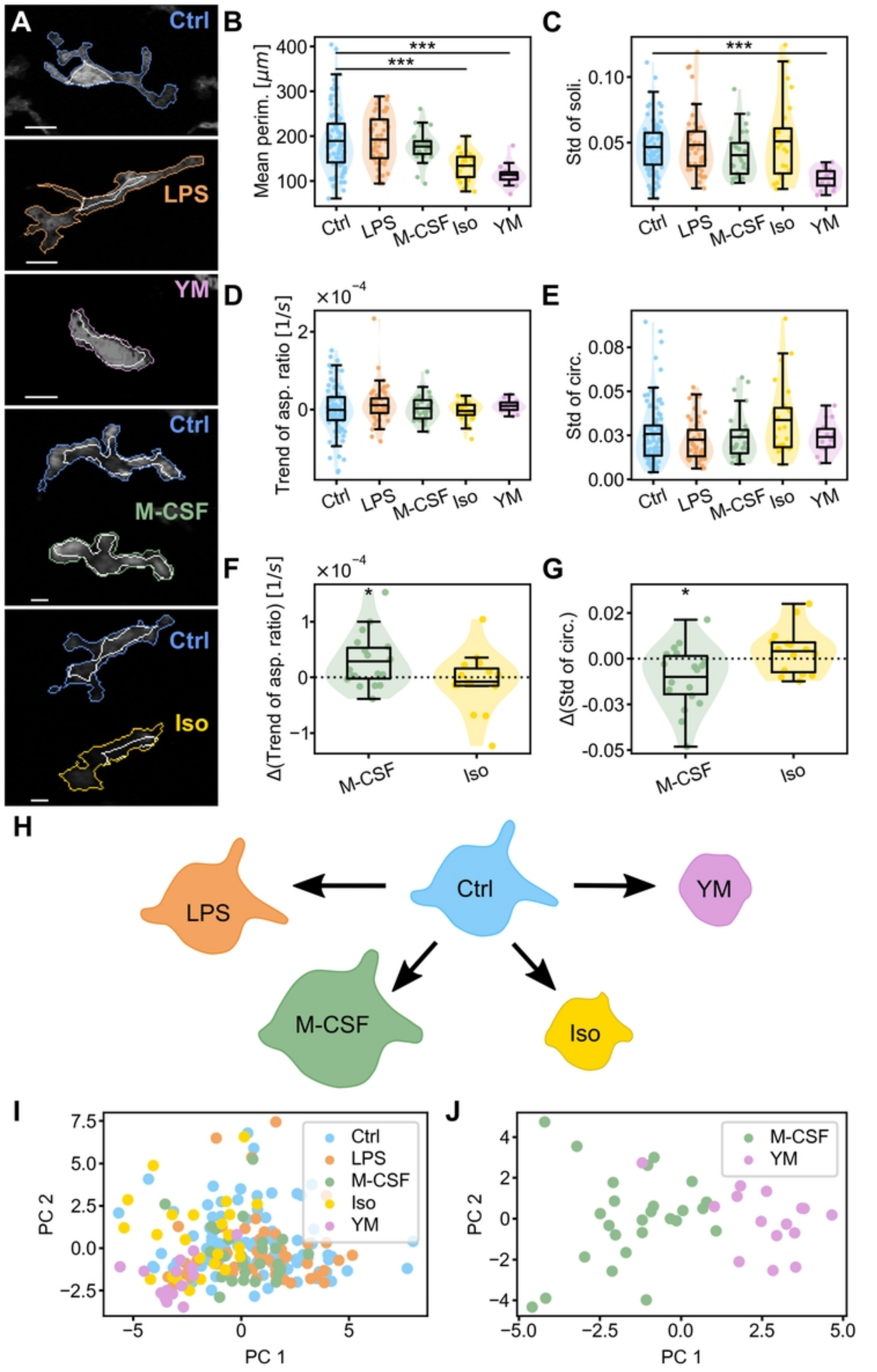
A
Ctrl
LPS
YM
Ctrl
M-CSF
Ctrl
Iso
B
Mean perim. [μm]
400
300
200
100
***
***
Ctrl
LPS
M-CSF
Iso
YM
C
Std of soli.
0.10
0.05
***
Ctrl
LPS
M-CSF
Iso
YM
D
Trend of asp. ratio [1/s]
×10⁻⁴
2
0
Ctrl
LPS
M-CSF
Iso
YM
E
Std of circ.
0.08
0.05
0.03
0.00
Ctrl
LPS
M-CSF
Iso
YM
F
Δ(Trend of asp. ratio) [1/s]
×10⁻⁴
1
0
−1
*
M-CSF
Iso
G
Δ(Std of circ.)
0.02
0.00
-0.03
-0.05
*
M-CSF
Iso
H
Ctrl
LPS
YM
M-CSF
Iso
I
PC 2
7.5
5.0
2.5
0.0
−2.5
−5
0
5
PC 1
Ctrl
LPS
M-CSF
Iso
YM
J
PC 2
4
2
0
−2
−4
−5.0
−2.5
0.0
2.5
5.0
PC 1
M-CSF
YM

Figure 3

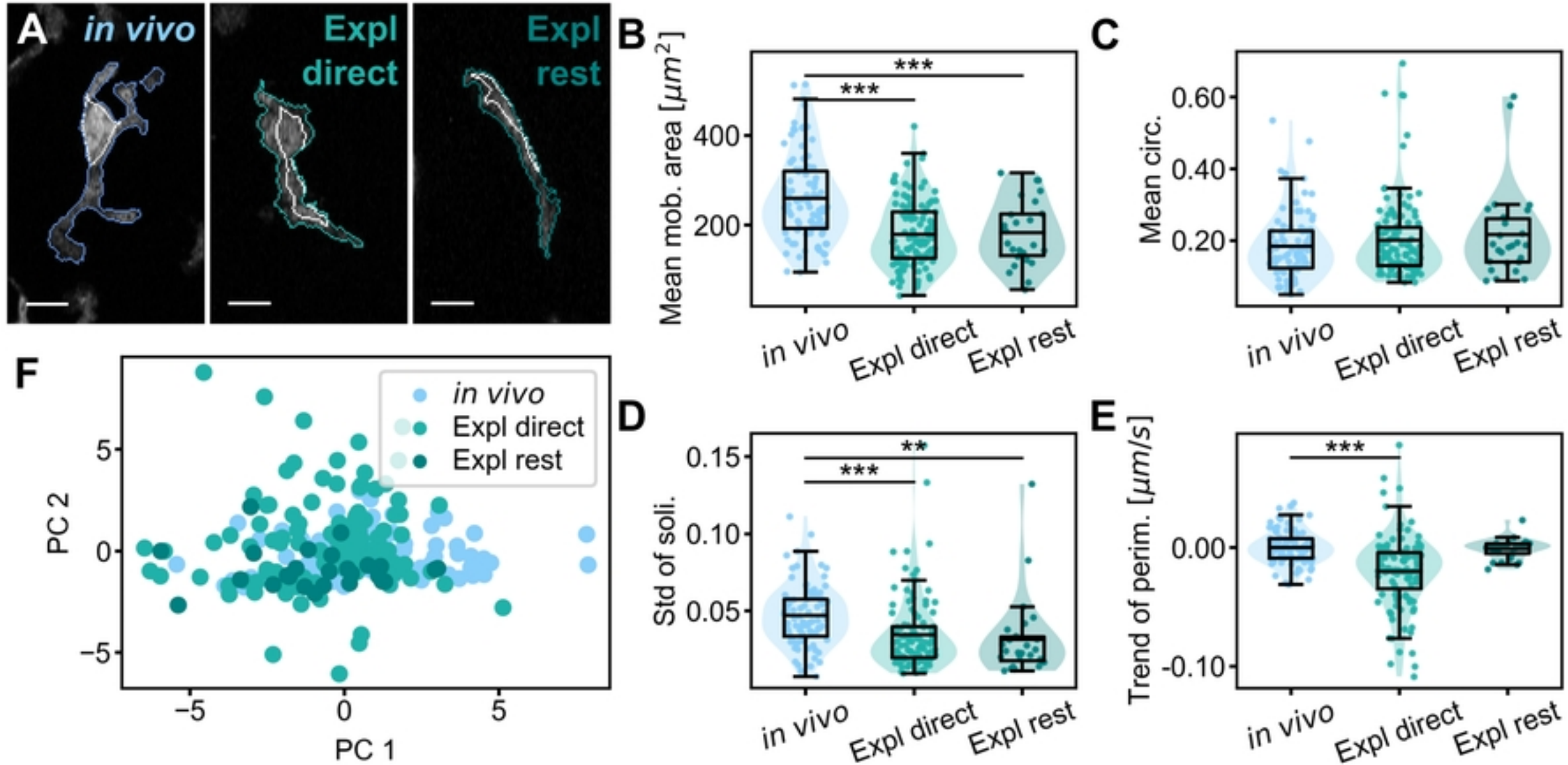
A
in vivo
Expl direct
Expl rest
B
Mean mob. area [μm²]
400
200
***
***
in vivo
Expl direct
Expl rest
C
Mean circ.
0.60
0.40
0.20
in vivo
Expl direct
Expl rest
D
Std of soli.
0.15
0.10
0.05
**
***
in vivo
Expl direct
Expl rest
E
Trend of perim. [μm/s]
0.00
-0.10
***
in vivo
Expl direct
Expl rest
F
in vivo
Expl direct
Expl rest
PC 2
PC 1
5
0
−5
−5
0
5

Figure 4

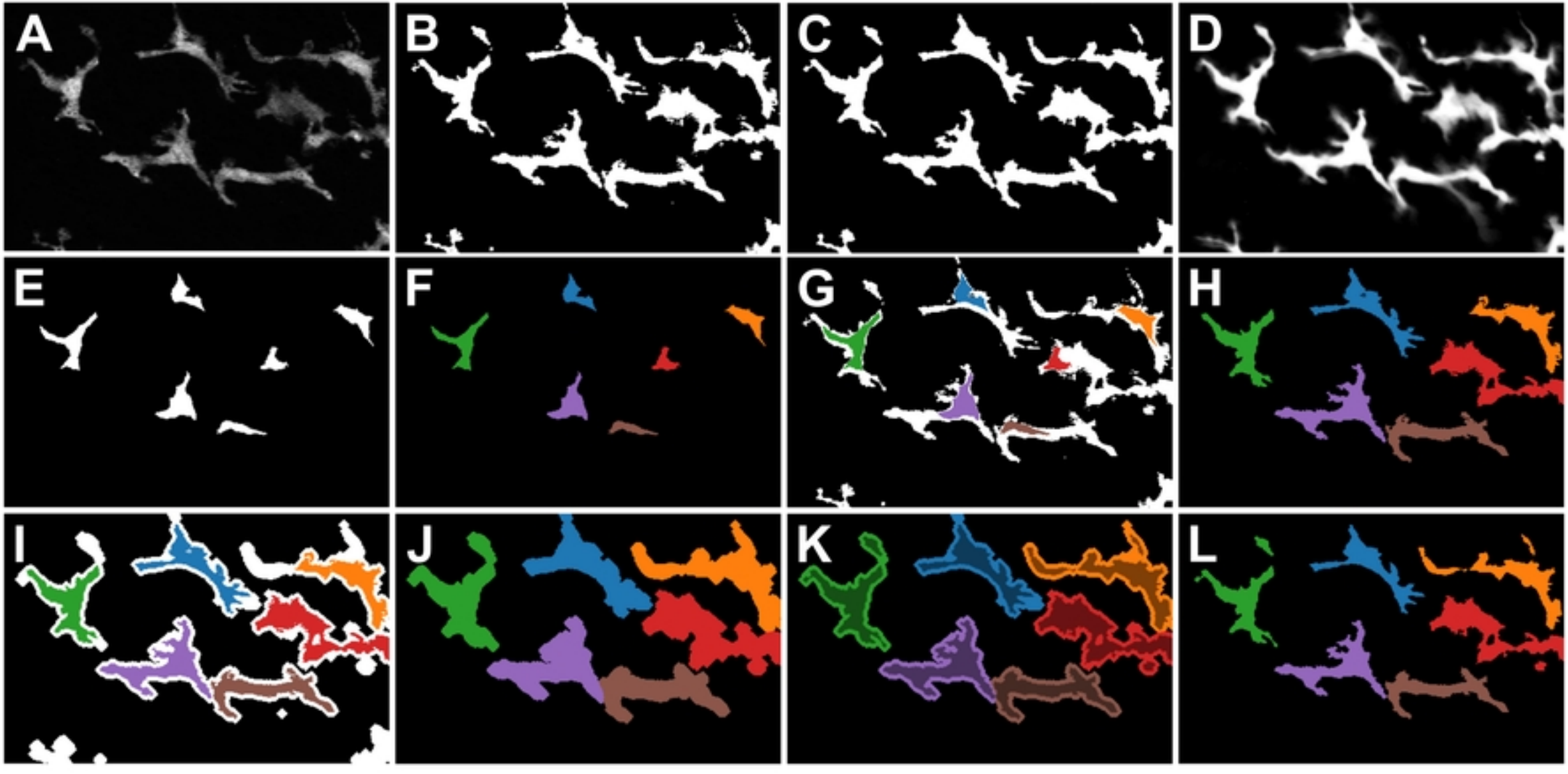

Figure 5